Contents lists available at ScienceDirect

# Bioactive Materials

# Bioinspired super-hydrophilic zwitterionic polymer armor combats thrombosis and infection of vascular catheters

You Ke [a,b,1], Haotian Meng [a,b,1], Zeyu Du [a,b,1], Wentai Zhang [a], Qing Ma [a,b], Yuting Huang [a], Linxian Cui [c,***], Yifeng Lei [d,**], Zhilu Yang [a,b,*]

[a] *Dongguan Key Laboratory of Smart Biomaterials and Regenerative Medicine, The Tenth Affiliated Hospital, Southern Medical University, Dongguan, Guangdong, 523000, China*
[b] *School of Materials Science and Engineering, Key Lab of Advanced Technology for Materials of Education Ministry, Southwest Jiaotong University, Chengdu, Sichuan, 610031, China*
[c] *Geriatric Diseases Institute of Chengdu/Cancer Prevention and Treatment Institute of Chengdu, Department of Cardiology, Chengdu Fifth People's Hospital (The Second Clinical Medical College, Affiliated Fifth People's Hospital of Chengdu University of Traditional Chinese Medicine), Chengdu, Sichuan, 611137, China*
[d] *The Institute of Technological Science, Wuhan University, Wuhan, 430072, China*

## ARTICLE INFO

## ABSTRACT

Thrombosis and infection are two major complications associated with central venous catheters (CVCs), which significantly contribute to morbidity and mortality. Antifouling coating strategies currently represent an efficient approach for addressing such complications. However, existing antifouling coatings have limitations in terms of both duration and effectiveness. Herein, we propose a durable zwitterionic polymer armor for catheters. This armor is realized by pre-coating with a robust phenol-polyamine film inspired by insect sclerotization, followed by grafting of poly-2-methacryloyloxyethyl phosphorylcholine (pMPC) via *in-situ* radical polymerization. The resulting pMPC coating armor exhibits super-hydrophilicity, thereby forming a highly hydrated shell that effectively prevents bacterial adhesion and inhibits the adsorption and activation of fibrinogen and platelets *in vitro*. In practical applications, the armored catheters significantly reduced inflammation and prevented biofilm formation in a rat subcutaneous infection model, as well as inhibited thrombus formation in a rabbit jugular vein model. Overall, our robust zwitterionic polymer coating presents a promising solution for reducing infections and thrombosis associated with vascular catheters.

## 1. Introduction

Central venous catheters (CVCs) significantly enhance the current clinical efficiency by providing sustained vascular access for the administration of nutrition [1], antibiotics [2] and drugs [3]. However, their usage is often accompanied by complications such as thrombosis and infection [4,5]. Firstly, blood components can adhere to these catheters, triggering coagulation and thrombus formation [6]. In addition, catheters can act as conduits for bacterial entry, leading to microbial growth on their surfaces and biofilm formation [7,8]. Clinically,

the administration of anticoagulants [9] and antibiotics [10] is the typical method to address these issues. Nonetheless, their extensive use may cause severe adverse effects, like hypersensitivity and heparin-induced thrombocytopenia [11], and the emergence of antibiotic-resistant bacteria [12–14]. Furthermore, the long-term indwelling of catheters increases the risk of these complications occurring simultaneously. Increasing evidence suggests a pathophysiological relationship between thrombus formation and biofilm growth on the surface of catheters [15–17]. Proteins in thrombi, such as fibronectin and fibrin, are conducive to bacterial adhesion, facilitating the

development of biofilms. In turn, the presence of these biofilms can induce platelet aggregation, exacerbating thrombus accumulation. Therefore, it is essential to endow catheters with both enhanced anti-coagulant and antibacterial properties.

Recently, antifouling surfaces have emerged as a promising strategy to combat both thrombosis and infection of vascular catheters [18–20]. Zwitterionic polymers, in particular, are increasingly recognized as effective molecules for creating antifouling surfaces [21,22]. Their unique molecular structure, characterized by large dipole moments and numerous ionic groups, enables these polymers to form a dense hydration shell on the surface to repel biofouling [23,24]. This feature is particularly promising for CVCs, as it effectively reduces the adsorption of proteins, bacteria and cells, potentially achieving thromboprotection and anti-infective properties simultaneously.

Zwitterionic polymers are commonly immobilized on the surfaces of CVCs by grafting technologies, which can be divided into two approaches: (i) 'grafting to' strategy, involving the direct integration of end-functionalized zwitterionic polymers onto the surface; (ii) 'grafting from' strategy, which enables the *in-situ* polymerization of zwitterionic

monomers on the pre-activated surface [25]. However, both methods have limitations. For the 'grafting to' strategy, the steric hindrance caused by macromolecular chains impedes the dense grafting of zwitterionic polymers. Surface grafting density has been shown to impact the antifouling characteristics of surfaces [26,27]. For the 'grafting from' strategy, the inert surfaces of CVCs lack the necessary active sites required for the covalent binding with zwitterionic monomers [28]. Therefore, surface pre-activation becomes a crucial step before grafting. Nonetheless, achieving uniform and stable activation of the cylindrical surfaces on CVCs poses a significant challenge.

Herein, we propose a robust and amine-rich priming coating as a platform for dense, uniform and stable grafting of zwitterionic polymers to endow the catheters with excellent antifouling capabilities. This technique is inspired by the process of insect cuticle sclerotization, which involves the crosslinking of cuticular proteins (polyamine) and phenolic compounds (phenol) mediated by phenol oxidases and the oxygen at the cuticle-air interface (Fig. 1A, left). Initially, we synthesized a hydrogenated caffeic acid (HCA, 3-(3,4-dihydroxyphenyl) propionic acid)-conjugated polyallylamine (PA) as a fundamental
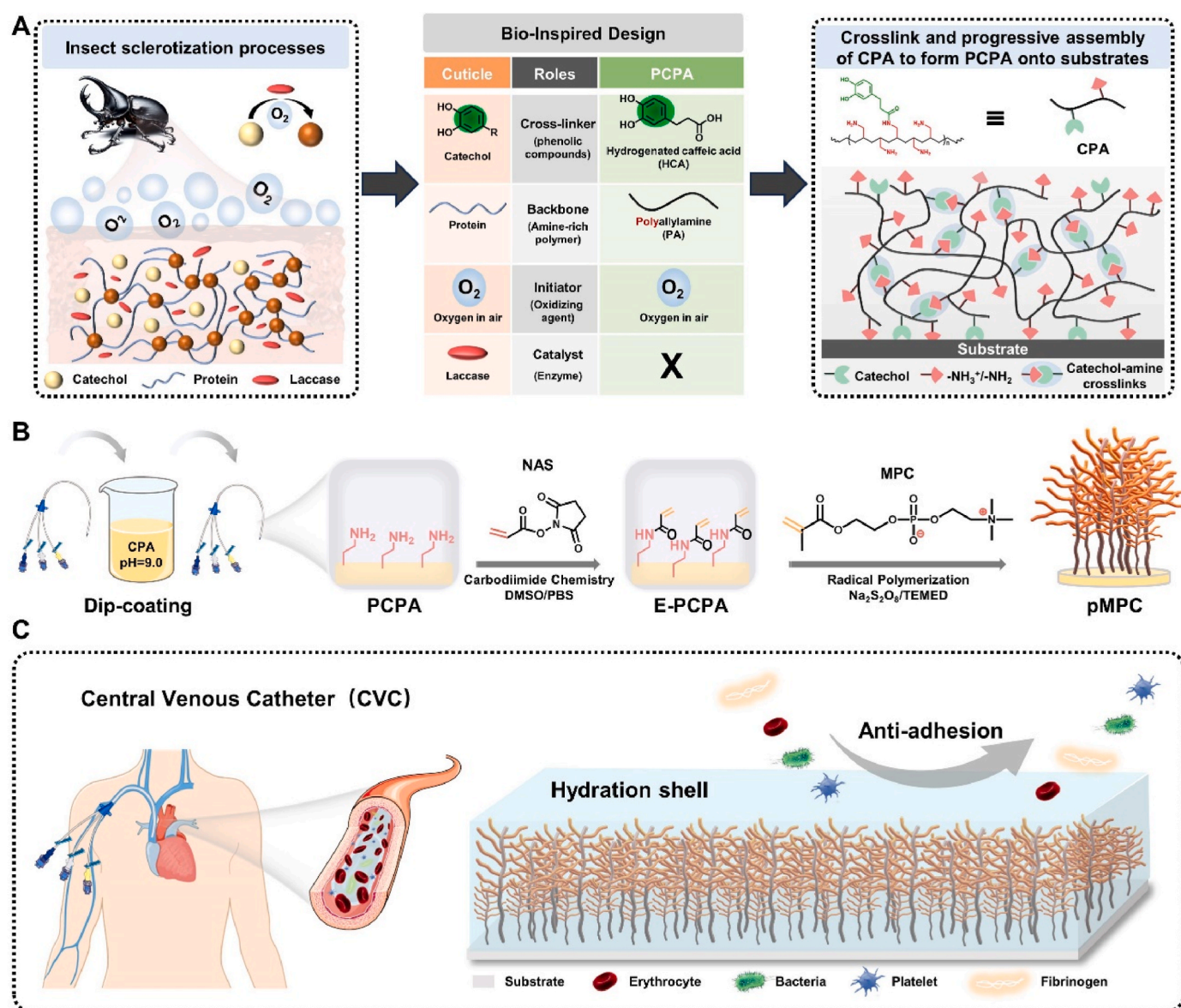


**Fig. 1.** Mimicking the insect cuticle sclerotization process for developing pMPC armor. (A) Insect cuticle sclerotization process (left) and formation mechanism of adhesive armor PCPA (right). (B) Construction of pMPC armor through carbodiimide chemistry and free radical polymerization. (C) Illustration of the antifouling properties of pMPC armor.

component (CPA). Then, the CPA molecules crosslinked among themselves in the presence of air oxygen through phenol-polyamine chemistry, forming a robust and adhesive polymerized CPA (PCPA) coating with abundant active groups on its surface (Fig. 1A, right). Subsequently, N-Succinimidyl acrylate (NAS) was grafted onto the PCPA layer via carbodiimide chemistry, introducing the carbon-carbon double bonds. Finally, the poly-2-methacryloyloxyethyl phosphorylcholine (pMPC) molecular brushes were robustly grafted onto the surface through *in-situ* radical polymerization (Fig. 1B). This process results in a dense grafting of pMPC and super-hydrophilicity of the grafted surface, which is expected to impart catheters with remarkable anti-adhesion properties. (Fig. 1C). Overall, this innovative design of a super-hydrophilic armor provides an effective method to prevent both thrombus and biofilm formation on catheters. This advancement holds significant potential for improving the safety and efficacy of catheters in clinical settings.

## 2. Materials and methods

### 2.1. Materials

HCA, PA (Mw ~17,000), N-3-dimethylaminopropyl)-N′-ethylcarbo (EDC), N-hydroxysuccinimide (NHS), 2-Morpholinoethanesulfonic acid monohydrate (MES) were purchased from Sigma. N,N,N′,N′-Tetramethylethylenediamine (TEMED), sodium hydroxide (NaOH), NAS, 2-Methacryloyloxyethyl phosphorylcholine, acid orange II (AO II), Sodium persulfate ($Na_2S_2O_8$) were purchased from Aladdin. Hydrochloric acid (HCl), Dimethyl sulfoxide (DMSO), phosphate buffered saline (PBS) were provided by Chengdu Kelong Chemical Reagents Co., Ltd. (Chengdu, China).

### 2.2. CPA synthesis

The synthesis of CPA involved a carbodiimide chemistry process. Initially, HCA was activated using EDC (3 equivalents to HCA) and NHS (1 equivalent to HCA) in MES buffer solution (pH 5.6) for 30 min at 37 °C. Following this, PA was introduced into the mixture, and the reaction was allowed to proceed for 24 h at 10 °C. To prevent the oxidation of phenolic hydroxyl groups, the entire process was conducted in an anaerobic environment protected with nitrogen gas ($N_2$). Subsequently, the mixture was purified by dialysis in anaerobic ultrapure water with a molecular weight cutoff of 1000 for 48 h at 4 °C, with the water being renewed every 6 h. Finally, the resulting CPA was then freeze-dried for preservation.

### 2.3. Preparation of PCPA coatings

CPA (0.2 mg/mL) was dissolved in ultrapure water and the pH was adjusted to 9 using 1 mM NaOH. The substrates were immersed in the solution for 24 h at 37 °C, then washed with ultrapure water under ultrasound and dried with $N_2$. The obtained samples were labelled as PCPA. To achieve a uniform and dense coating, the deposition process was repeated three times.

### 2.4. Preparation of E-PCPA and MPC surface

First, NAS (3 mg/mL) was dissolved in a mixed solvent consisting of 95 % PBS and 5 % DMSO. The PCPA coated substrates were then immersed in this solution for 12 h at 25 °C. Subsequently, the substrates were washed with ultrapure water, dried with $N_2$, and labelled as E-PCPA. Following that, the E-PCPA were immersed in a mixed solution containing MPC (100 mg/mL), $Na_2S_2O_8$ (10 mg/mL), and TEMED (4 μL/mL) for 48 h under an $N_2$ environment. After grafting, the substrates were washed with ultrapure water, dried with $N_2$, and labelled as pMPC.

### 2.5. Characterization

The $^1H$ nuclear magnetic resonance ($^1H$ NMR) spectrum was obtained by AV II-400 (Bruker, Germany). The chemical structure was determined using Fourier Transform infrared spectroscopy (FTIR) (Nicolet 5700, USA). The ultraviolet–visible (UV–vis) spectrum was obtained by TU-1901 (China). Surface topography was recorded using a camera (Z7II, Nikon Ltd., Japan) and scanning electron microscopy (SEM) (JSM-6390, JEOL, Japan). Surface elemental composition was measured using X-ray Photoelectron Spectroscopy (XPS) (ESCALAB 250Xi, Thermo Fisher, USA). Thickness and water contact angle (WCA) were determined using ellipsoid polarization spectrometer (M − 2000 V, J.A. Woollam, USA) and Krüss GmbH DSA 100 Mk 2 goniometer (Hamburg, Germany), respectively.

### 2.6. Coefficient of friction

The coefficient of friction (COF) was measured using a scanning probe microscope (AFM/SPM, E-WEEP, Nanocute, Japan). To simulate the wet condition of practical application, PBS was used as the lubricant during the measurement. The friction tests were performed across a range of loads, spanning from 50 to 250 nN, which was equivalent to the maximum contact pressures of 27.3 MPa (50 nN), 39.4 MPa (150 nN), and 46.7 MPa (250 nN), respectively. Scan rates were adjusted within 1–3 Hz range, ensuring a constant sliding distance of 20 μm.

### 2.7. Quantification of amino groups

The acid orange colorimetric method was employed to investigate the density of amine groups on the surface. In brief, the samples were immersed in an AO II solution (3.5 mM, pH 3) for 12 h at 37 °C. Subsequently, the samples were rinsed with HCl solution (pH 3) to remove unreacted AO II and dried with $N_2$. Following this, NaOH solution (200 μL, pH 12) was applied to the sample surface for 15 min to release AO II. The concentration of AO II in the NaOH solution was measured at 485 nm using an enzyme marker (μQuant, Bio-Tek Instruments Inc.).

### 2.8. Antibacterial activity in solid medium

The antibacterial experiment was conducted using Gram-positive *Staphylococcus epidermidis (S. epidermidis)* and Gram-negative *Escherichia coli* (*E. coli*) following the ISO 22196-2011 standard. Initially, bacteria were cultured on solid agar medium at 37 °C for 24 h. Bacterial colonies consisting of 1–2 rings was then transferred into a bacterial nutrient solution consisting of 1 % liquid culture medium and 99 % physiological saline, followed by incubation at 37 °C for 24 h. *E. coli* and *S. epidermidis* were diluted to concentrations ranging from $5 \times 10^5$ to $1 \times 10^6$ CFU/mL using the nutrient solution. Subsequently, 100 μL of the standardized bacterial suspension was evenly dispersed onto the sample surfaces, covered with sterile polyethylene film, and incubated at 37 °C for 24 h. To assess antibacterial activity in solid medium, bacteria on the sample surfaces were rinsed and diluted with 1 mL of physiological saline. Then, 20 μL of the bacterial suspension was spread onto solid medium and further incubated for 24 h. The growth conditions of bacteria were observed using a camera and SEM, and bacterial counts were conducted using Image J software. To further analyze the antibacterial mechanism, a live/dead bacterial staining assay was performed. The antibacterial rate was calculated using Formula (1).

The formula for calculating the antibacterial rate is as follows:

$$R = (T_C - T) / T_C \times 100\% \tag{1}$$

Where $T_C$ and $T$ represent the colony count of the control group and the samples, respectively.

## 2.9. Cell compatibility

The sterilized samples were immersed in DMEM/F12 medium supplemented with 10 % FBS at a ratio of 3 mL/cm$^2$ for the cell culture medium volume to the surface area of the coating. After 72 h incubation in a cell culture incubator (5 % $CO_2$, 37 °C), the extracts were collected for cell culture. Human umbilical vein endothelial cells (HUVECs) were first seeded at a density of $2 \times 10^4$ cells/cm$^2$ in a well plate. After 24 h of incubation, the cell culture medium was replaced with 1 mL of the extract for further incubation of 24 and 72 h. Then the cell viability was assessed using a CCK-8 assay. HUVECs were purchased from the GuangZhou Jennio Biotech Co., Ltd.

## 2.10. In vitro antifouling properties against fibrinogen

Fresh whole blood was obtained from adult New Zealand White rabbits, and all blood samples were anticoagulated with 3.8 % sodium citrate (volume ratio of 9:1). Whole blood was centrifuged to obtain platelet-rich plasma (PRP, centrifuged at 1500 rpm for 15 min) and platelet-poor plasma (PPP, centrifuged at 3000 rpm for 10 min). To evaluate the anticoagulant properties of the pMPC surface, the adhesion and activation of fibrinogen (Fg) and platelets were assessed.

For the Fg adhesion experiment, 300 μL of PPP was added to the sample surface, incubated at 37 °C for 2 h, and then rinsing with physiological saline. After blocking with BSA for 30 min and rinsing, 200 μL of horseradish peroxidase (HRP)-labelled Fg antibody was added and incubated at 37 °C for 30 min. Subsequently, 3,3′,5,5′-tetramethylbenzidine (TMB) chromogenic substrate solution was added. After incubation at 37 °C for 20 min, 100 μL of 1 mol/L sulfuric acid stop solution was added, and the absorbance was finally measured at 450 nm.

For the analysis of Fg activation, after incubating 300 μL of PPP on the sample surface for 2 h, 200 μL of γ-Fg monoclonal antibody working solution was added and incubated at 37 °C for 1 h. After rinsing, 200 μL of HRP labelled polyclonal antibody was added, and the reaction was carried out for 30 min. Subsequently, a solution of TMB was added and incubated for 20 min. Finally, sulfuric acid stop solution was added, and the absorbance was measured at 450 nm.

## 2.11. Anti -adhesion and -activation properties against platelets

The adhesion and activation of platelets on the sample surface were quantitatively analysed by measuring the expression of P-selectin and lactate dehydrogenase (LDH). Initially, 300 μL of PRP was added to the sample surface and incubated at 37 °C for 1 h, following by washing with PBS. Subsequently, lysis was performed using Triton X-100 (10 % v/v), and the LDH content in the lysate was detected using an LDH Elisa kit (Rabbit, 69–77499, Wuhan MSK Biotechnology Co., Ltd.). The determination of P-selectin content followed the same protocol as the LDH evaluation and was finally assessed using a P-selectin Elisa kit (Rabbit, 69–22260, Wuhan MSK Biotechnology Co., Ltd.). To observe the adherent platelets on the samples, 0.5 mL of PRP was added to the surface and incubated for 30 min at 37 °C. After the incubation, the sample surface was rinsed with physiological saline, followed by fixation with 2.5 wt% glutaraldehyde. Subsequently, dehydration was performed using a gradient of ethanol concentrations (50 %, 75 %, 90 %, and 100 %). The samples were then subjected to gold sputtering and observed using SEM.

## 2.12. Hemolysis test

The whole blood was diluted with physiological saline (samples and negative control group) or ultrapure water (positive control group) at a volume ratio of 4:5. After incubating at 37 °C for 1 h, the absorbance at 540 nm was measured using an enzyme marker. The hemolysis rate was calculated using the following formula (2):

$$\text{Hemolysis Rate (\%)} = (OD_M - OD_1)/(OD_2 - OD_1) \times 100\% \tag{2}$$

Where, $OD_M$, $OD_1$, $OD_2$ is the absorbance value of the experimental group, the negative control, and the positive control, respectively.

## 2.13. Ex vivo anti-thrombogenicity

The animal experiment was approved by the Animal Welfare and Ethics Committee of the Tenth Affiliated Hospital of Southern Medical University (Approval Number: IACUC-AWEC-202211015). All the animals used in this study were euthanized by anesthetic overdose. To evaluate the antithrombotic effect of the coatings, an *ex vivo* blood circulation experiment was conducted using adult New Zealand White rabbits weighing between 2.5 and 3.0 kg. Pentobarbital sodium was employed to aesthesia animals at a concentration of 30 mg/mL, with a dosage of 1 mL per kg. The left carotid artery and right external jugular vein of rabbits were surgically exposed and cannulated. Subsequently, the bare and modified silicone rubber (SR) catheters were connected to the cannulas to form a four-channel extracorporeal circulation loop. Four New Zealand White rabbits were used for this experiment. After 2 h of *ex vivo* circulation, the catheters were removed and rinsed with physiological saline. Then, physiological saline was pumped into the catheter at a certain pressure to measure the post-circulation blood flow rate. After drying, the weight of thrombus formed in the catheters was measured. Additionally, cross-sectional photographs of the catheter lumen were taken, and the occlusion rate was calculated. Thrombus on the luminal surface of the catheter was observed by SEM.

## 2.14. Blood analysis by ex vivo blood circulation

During different time intervals (0, 5, 30, 60 min) of *ex vivo* blood circulation, blood samples were collected for routine blood and biochemical tests. To better simulate clinical practice, an extended tube with a length of 1.6 m and an inner diameter of 3 mm was used to increase the contact area between blood and the material surface. Four New Zealand White rabbits were used for each of bare and pMPC-armored catheters. After collection, blood tests were conducted, including activated prothrombin fragment 1 + 2 (F1+2), partial thromboplastin time (APTT), platelet count (PLT), complement component 3a (C3a), C-reactive protein (CRP), white blood cell count (WBC), interleukin-10 (IL-10), tumor necrosis factor-alpha (TNF-α), alanine aminotransferase (ALT) and creatinine (CREA). APTT was measured using the APTT kit (ellagic acid, coagulation method, E118, Shanghai Sun Biotechnology Co.). WBC and PLT counts were measured using an animal automatic blood cell analyzer (Shenzhen Mindray, BC-2800Vet), ALT and CREA levels were assessed using an animal biochemical analyzer (Shenzhen Mindray, BS-240VET).

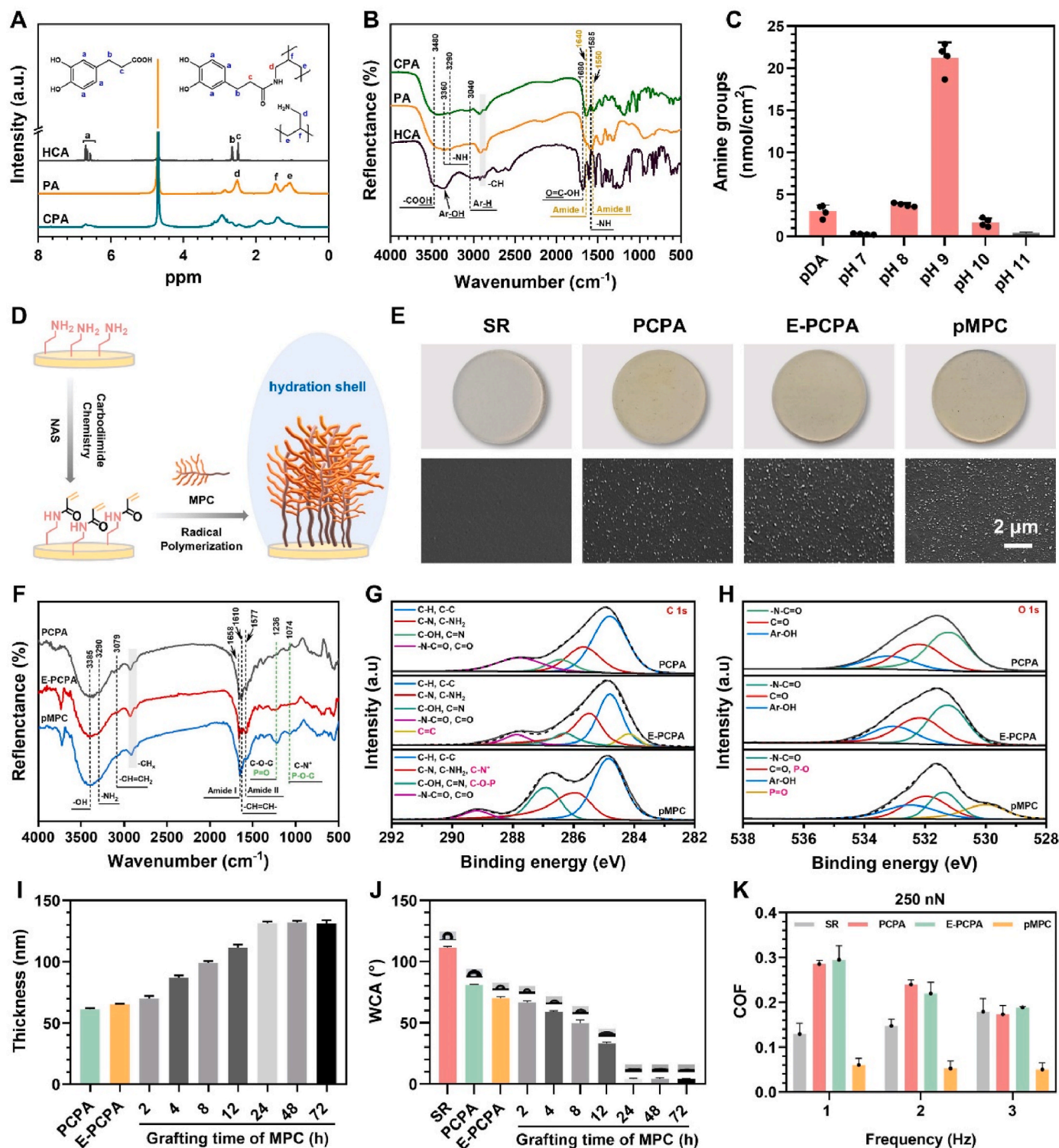## 2.15. Long-term stability of the pMPC surfaces

To evaluate the long-term antibacterial and antithrombotic properties of the pMPC surface, samples were immersed in PBS solution at 37 °C for a continuous period of 30 days. After immersion, the samples were washed at least three times, followed by drying with $N_2$ for further analysis. Samples were characterized at different time points (1, 3, 7, 15, 30 days) to assess various parameters, including thickness, WCA, antibacterial and *ex vivo* anticoagulant performance. Four New Zealand White rabbits were utilized for the *ex vivo* anticoagulant test. Additionally, immersion solutions at different time points were subjected to inductively coupled plasma mass spectrometry (ICP-MS) to assess the phosphorus element content in the solution.

## 2.16. Inflammation studies with CVCs samples exposed to bacteria

Aseptic CVC samples were cut into 2 cm slices. *S. epidermidis* and

*E. coli* were diluted to a concentration of $5 \times 10^5$–$1 \times 10^6$ CFU/mL using nutrient solution. The samples were exposed to the bacteria solution for 24 h at 37 °C. Then the samples were collected and placed in physiological saline at room temperature for approximately 2 h. Afterwards, the samples were inserted into subcutaneous pockets on the backs of

Sprague-Dawley (SD) rats, and the wounds were sutured with surgical thread. Four SD rats were used for each bacterial strain, namely *E. coli* and *S. epidermidis*. After 7 days implantation, the samples were removed for photography and hematoxylin and eosin (H&E) staining.



**Fig. 2.** Preparation and characterization of PCPA armor and pMPC armor. (A) $^1$H NMR spectrum of HCA, PA and CPA. (B) FTIR spectra of HCA, PA and CPA. (C) Surface density of amine groups in PCPA coatings fabricated using CPA in solutions pH-adjusted to 7–11. (D) Schematic illustration of MPC grafting on PCPA surface. (E) Photographs and SEM images of SR, PCPA, E-PCPA and pMPC. (F) FTIR spectra of PCPA, E-PCPA and pMPC. Peak-fitting XPS spectra of (G) C1s and (H) O1s for PCPA-modified SR before and after grafting with NAS and MPC. Changes in (I) thickness and (J) WCA after MPC grafting onto E-PCPA (K) COF of SR, PCPA, E-PCPA and pMPC surface under the load of 250 nN.

### 2.17. In vivo thrombogenicity of pMPC modified CVCs

Eight New Zealand White rabbits were anesthetized, and pMPC-modified and commercial CVCs were inserted approximately 10 cm into the jugular vein from the neck. Catheters were secured and wounds were closed. After about 8 h, animals were euthanized and jugular vein with catheters in place were explanted for observation.

### 2.18. Statistical analysis

The data were represented as the mean with standard deviation, and all the experiments were repeated at least three times unless indicated otherwise. Statistical analyses were carried out using Student's t-test and one-way analysis of variance (ANOVA). The analyses were performed using GraphPad Prism 9.0 (GraphPad Software, Inc., San Diego, USA).

## 3. Results and discussion

### 3.1. Preparation and characterization of super-hydrophilic zwitterionic polymer coating armor

We initially synthesized a hydrogenated caffeic acid-conjugated polyallylamine as a fundamental component (CPA). To maintain the activity of the phenolic hydroxyl groups in HCA, the reaction was conducted under anaerobic acidic conditions. Subsequently, we characterized the physicochemical properties of CPA. The $^1$H NMR spectrum revealed diagnostic peaks containing both aromatic protons from HCA and amino protons from PA, confirming the successful connection between HCA and PA (Fig. 2A). FTIR further confirmed the synthesis of CPA through EDC/NHS chemistry between HCA and PA. As depicted in Fig. 2B, the characteristic peaks of HCA (e.g., the peaks of Ar-OH and Ar–H at 3350 and 3040 cm$^{-1}$, respectively) and PA (e.g., the peaks of N–H stretching vibrations at 3360 and 3290 cm$^{-1}$) were observed in the spectra of CPA. Notably, the –COOH peak at 3480 cm$^{-1}$ disappeared, and stretching vibration peaks corresponding to Amide I and Amide II appeared at 1640 cm$^{-1}$ and 1550 cm$^{-1}$, respectively. This was further supported by UV–Vis analysis (Fig. S1), where visible benzene ring absorption peaks were clearly detected at 280.1 nm and 287.4 nm in the spectra of HCA and CPA, respectively. The significant redshift in the benzene ring absorption peak was observed in CPA due to the auxochrome group (-NH$_2$) attached to HCA, which shifts the absorption to a longer wavelength [29].

We further explored the feasibility of film formation for the synthesized CPA and its affinity for subsequent grafting of MPC. The density of amine groups on the surface was determined using acid orange II colorimetric method. The results indicated that the PCPA film achieved the highest amine density of 21.2 nmol/cm$^2$ at a pH of 9, which is notably higher than that of the Polydopamine (pDA) coating (Fig. 2C). This highlighted the potential of the obtained PCPA coating to function as an amine-rich platform for subsequent MPC grafting to the surface via a two-step process. As illustrated in Fig. 2D, we initiated the grafting of NAS onto the surface of the PCPA coating through carbodiimide chemistry, introducing the carbon-carbon double bonds (E-PCPA). Subsequently, the substrate modified with E-PCPA was coated with pMPC molecular brushes using free-radical grafting and *in-situ* polymerization. The macroscopic images showed that, compared to SR, the coated substrates exhibited a light-yellow color, indicating the successful construction of these coatings (Fig. 2E). SEM micrographs further supported this, as the SR surface was smooth, whereas the coated surfaces exhibited numerous small particles. Before and after pMPC grafting, the nanoscale particles on the modified substrate surface were distributed uniformly and dense, demonstrating its potential for achieving a uniform coating on the CVCs surface.

FTIR and XPS were employed to analyze the chemical composition and structural changes of the modified SR further. In the FTIR spectrum of E-PCPA (Fig. 2F), a peak at 3079 cm$^{-1}$ appeared, corresponding to the

introduced C=C bond, indicating the successful fixation of NAS. The significant reduction in amine group density on the PCPA surface after NAS grafting also supported this observation (Fig. S2). After grafting with pMPC, the peaks at 1236 cm$^{-1}$ (C–O–C and P=O stretching vibrations) and 1074 cm$^{-1}$ (C–N$^+$ and P–O–C stretching vibrations) were observed, indicating the successful grafting and polymerization of pMPC on the surface of E-PCPA. XPS analysis further confirmed these results. The full spectrum of pMPC exhibited characteristic peaks of MPC at 191 eV and 133 eV, corresponding to P2s and P2p3, respectively (Fig. S3). The peak-fitting XPS spectra of C1s and O1s provided more detailed analysis of the presence of elements in the coating. In the C1s spectrum, a new peak was detected at 284.2 eV for E-PCPA, attributed to the carbon-carbon double bond in the NAS molecule. The changes in peaks at 286 eV and 286.9 eV for pMPC were considered contributions from C–N$^+$ and C–O–P in MPC, respectively. Moreover, the disappearance of the C=C peak suggested the successful immobilization of pMPC through free-radical grafting (Fig. 2G). The presence of peaks for P–O and P=O in the O1s spectrum of pMPC further verified the successful introduction of pMPC (Fig. 2H). Overall, these results corroborated the successful preparation of the pMPC-functionalized surface.

The antifouling effectiveness of zwitterionic polymer brushes exhibits a strong correlation with their thickness and grafting density [30]. Previous studies have found that when the thickness of the pMPC brush layer exceeds 5.5 nm $\pm$ 1 nm, it effectively reduces the adhesion of proteins and cells [31]. In our study, by utilizing the robust and amine-rich PCPA platform, zwitterionic polymer brushes with a thickness exceeding 65 nm and a grafting density of 254.62 µg/cm$^2$ (Fig. 2I and Fig. S4) were achieved after a polymerization time of 48 h. This thick and dense pMPC armor exhibited super-hydrophilic properties with a WCA of 4.1 $\pm$ 0.78° (Fig. 2J). Notably, the introduction of super-hydrophilic zwitterionic polymer brushes improved water-binding capability, leading to the formation of a stable hydration layer on the surface. Based on the water lubrication mechanism [32], this super-hydrophilic shell significantly reduces the friction coefficient (Fig. 2K and Fig. S5). This is advantageous for minimizing mechanical damage during the implantation process of central venous catheters.

### 3.2. In vitro antibacterial performance of the pMPC coating armor

The open skin wounds caused by the catheterization are prone to bacterial colonization from skin, consequently causing biofilms formation [33,34]. To evaluate the inhibitory effects of pMPC armor on bacterial adhesion, we selected representative strains, Gram-negative *E. coli* and Gram-positive *S. epidermidis*, for antibacterial experiments. As shown in Fig. 3A, the SR surface exhibited a substantial distribution of bacteria. Although PCPA and E-PCPA samples showed a slight reduction in bacterial colonization, the antibacterial effects were not significant. In contrast, pMPC armor demonstrated excellent antibacterial properties, with antibacterial rates of 99.77 $\pm$ 0.16 % and 99.58 $\pm$ 0.06 % for *E. coli* and *S. epidermidis*, respectively (Fig. 3B and C). SEM analysis and live/dead staining results further confirmed the robust antibacterial capabilities of the pMPC surface (Fig. 3D). It is noteworthy that PCPA and E-PCPA demonstrate modest antibacterial properties. The live/dead staining results showed bacteria with yellow staining on the surfaces of PCPA and E-PCPA. This could be attributed to the presence of positively charged amino groups or unsaturated fatty bonds in the coating, which impact the integrity of bacterial plasma membranes, thereby leading to the damage and death of bacteria [35]. Then the increased membrane permeability resulted in the partial penetration of the propidium iodide (PI) red fluorescence dye.

Cell compatibility is crucial for ensuring patient safety in practical applications. Therefore, we further examined the cytotoxicity of extracts from the pMPC armor on HUVECs. The CCK-8 assay and fluorescence imaging results demonstrated that the pMPC armor posed no risk of inducing cytotoxicity and did not adversely affect the proliferation and activity of endothelial cells (Fig. S6).
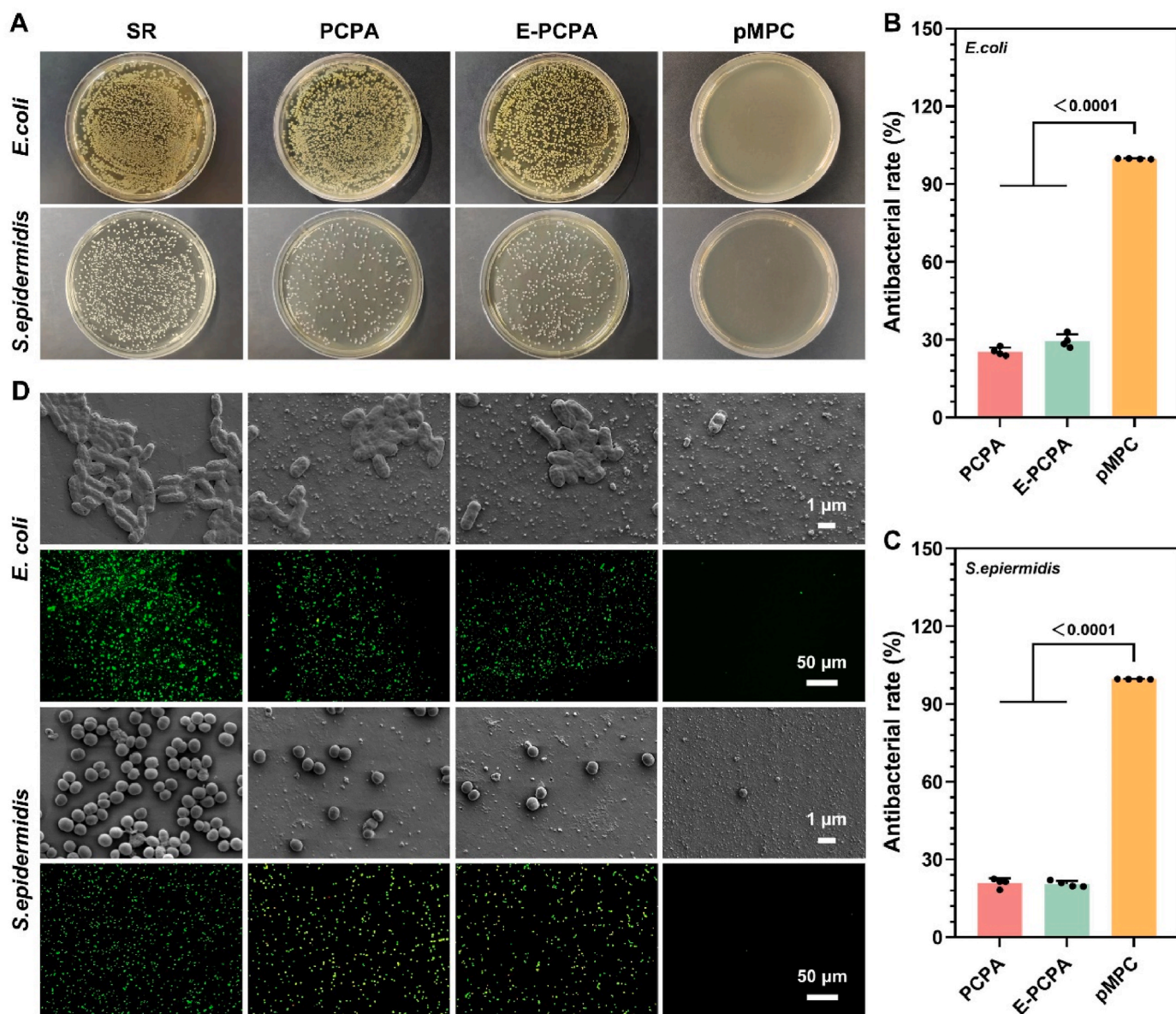
**Fig. 3.** Antibacterial properties of pMPC armor *in vitro*. (A) Typical *E. coli* and *S. epidermidis* colonies after 24 h incubation on bare and modified surface. Antibacterial rate of modified surface against (B) *E. coli* and (C) *S. epidermidis*. (D) SEM images and fluorescence microscopy images of *S. epidermidis* and *E. coli* on different samples. Data presented as mean ± SD (n = 4) and analysed using a one-way ANOVA.

### 3.3. In vitro antithrombotic properties of the pMPC coating armor

During the indwelling of CVCs, blood contact can lead to the adhesion of Fg on the surface. Subsequently, the adhered Fg further denatures and aggregates, converting into insoluble fibrin with the mediation of thrombin. Then aggregation of protofibrils into fibers results in the formation of a fibrin network that captures platelets, finally leading to coagulation [36,37]. Therefore, the adhesion and activation of Fg and platelets are two key factors of thrombus formation. Therefore, we first investigated the interaction between coated substrates and Fg using PPP. As shown in Fig. 4A, the PCPA coating induced the adhesion of Fg, which might be attributed to the electrostatic interaction between the positively charged amine groups on the PCPA surface and the negatively charged Fg [38]. In contrast, the pMPC surface significantly inhibited Fg adhesion, suggesting the antifouling properties of hydration armor formed by the polymer molecular brushes on the surface. In addition, the conformation of the adsorbed Fg is also crucial. Studies have shown that the carboxy-terminal end of the γ chain of fibrinogen plays a crucial

role in interacting with platelet integrin αIIbβ3, significantly contributing to platelet aggregation [39]. Therefore, we further evaluated the activity of the γ chain in the adsorbed Fg. The results were consistent with the adsorption test, showing a significant increase in the activity of the γ chain on the PCPA surface (Fig. 4B). In contrast, the pMPC surface exhibited significant inhibition of Fg activation. This demonstrates that the hydration armor formed by the polymer molecular brushes on the surface restricted the interaction between Fg and the surface.

Furthermore, we exposed the samples to PRP and quantitatively assessed the impact of different surfaces on platelet adhesion and activation using LDH and P-selectin assay kits, respectively. The results showed a significant increase in platelet adhesion on PCPA-modified surfaces, possibly attributed to the positively charged amine groups on the surface (Fig. 4C). Conversely, the pMPC armor exhibited a pronounced inhibitory effect on platelet adhesion. The activation state of platelets plays a crucial role in the coagulation process. Activated platelets secrete coagulation factors, expose phosphatidylserine, and facilitate the generation of thrombin and the formation of fibrin,
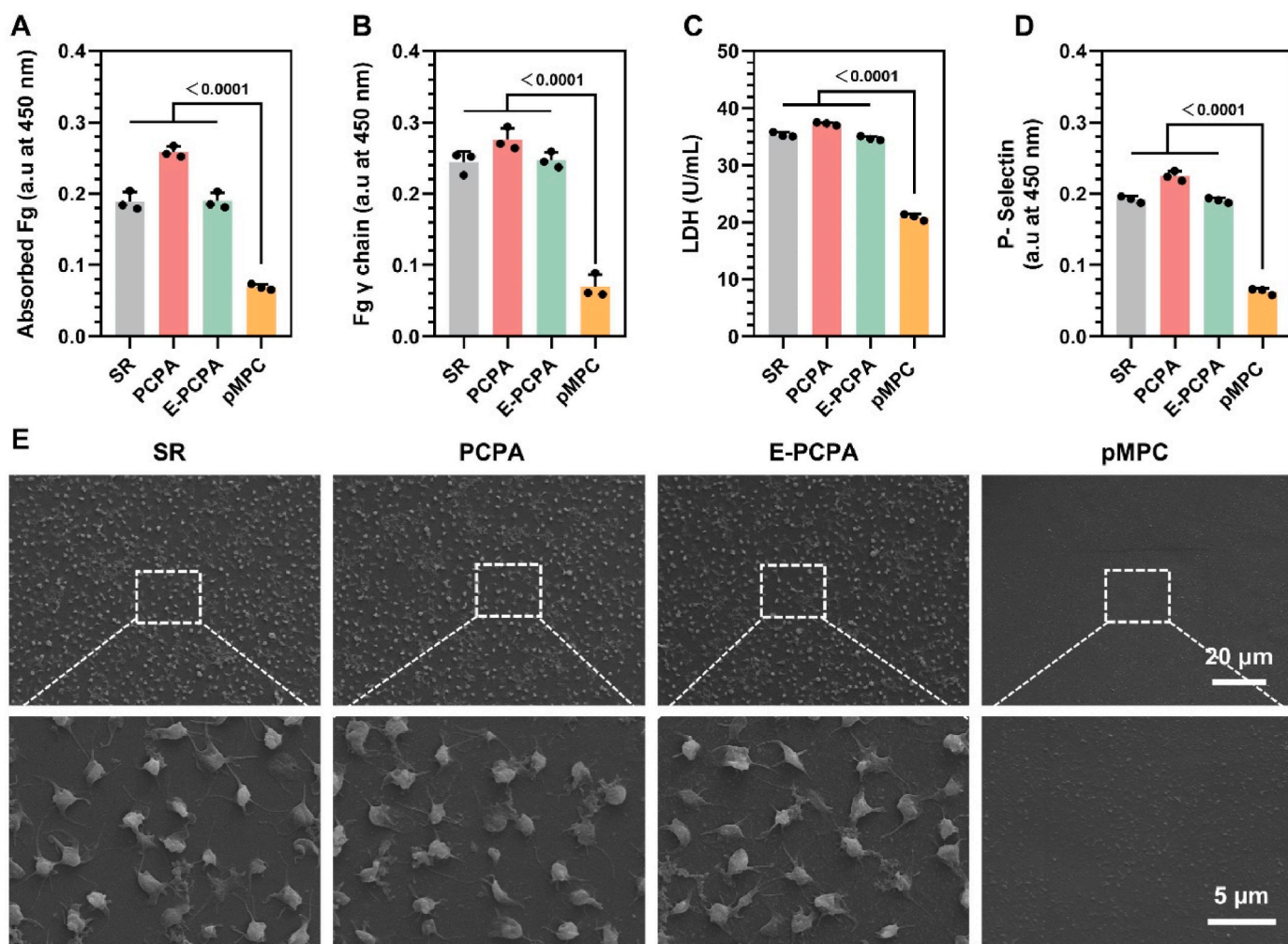
**Fig. 4.** Anti-thrombogenicity of pMPC armor *in vitro*. (A) Adsorbed and (B) activated fibrinogen on bare and modified surfaces. Quantitative results of platelet (C) adhesion and (D) activation on the modified SR substrate. (E) SEM images of platelets on different surfaces. Data presented as mean ± SD (n = 3) and analysed using a one-way ANOVA.

contributing to the progression of thrombus formation [40]. To assess the activation of adherent platelets, we conducted a quantitative analysis. Compared to SR groups, the number of active platelets on the pMPC surface showed a significant reduction. (Fig. 4D). SEM observation results were consistent with quantitative statistical results, the pMPC surface exhibited almost no adherent platelets, whereas the other samples showed a large number of activated platelets with extended filamentous pseudopodia on their surfaces (Fig. 4E). These findings demonstrated the effectiveness of the pMPC armor in preventing thrombus accumulation through the formation of a stable hydration shell on the surface. Moreover, as a surface-modified coating for blood-contacting devices, the pMPC armor demonstrated excellent blood compatibility with a hemolysis rate significantly lower than 5 %, meeting clinical use requirements (Fig. S7).

### 3.4. Ex vivo antithrombogenic properties of pMPC armored catheters

To further evaluate the antithrombotic performance of the pMPC armor, we conducted an *ex vivo* blood circulation experiment (Fig. 5A). The modified and unmodified SR catheters were connected to the left jugular vein and right carotid artery of rabbits to form an extracorporeal circulation loop. After 2 h of circulation, the catheters were removed, and occlusion ratio, thrombus weight, and blood flow rate were measured. Optical images revealed severe thrombus formation on the surface without pMPC grafting (Fig. 5B). In contrast, the pMPC surface

showed no apparent thrombus. SEM images further revealed that, in the absence of MPC, the surface exhibited a typical thrombus structure with platelets and red blood cells enveloped in a fibrin network, whereas the pMPC surface appeared notably clean with almost no thrombus formation (Fig. 5C). Quantitative analysis further confirmed the thromboresistant characteristics of the pMPC-armored surface. Specifically, the pMPC surface exhibited a significantly lower clotting rate (pMPC: 0.78 %, SR: 93.03 %, PCPA: 99.33 %, and E-PCPA: 94.38 %) and thrombus weight (pMPC: 774.75 mg, SR: 795.50 mg, PCPA: 848.00 mg, and E-PCPA: 7.75 mg) compared to other groups (Fig. 5D and E). Blood flow rate was also significantly improved for the pMPC group, which is consistent with the results observed in previous *in vitro* experiments (Fig. 5F).

Biomedical devices in direct contact with blood may influence the activation of relevant coagulation and inflammatory factors, potentially leading to adverse consequences such as thrombosis, inflammation [41] and organ functions [42]. In this study, we performed an additional *ex vivo* blood circulation experiment to evaluate the influence of our pMPC armor on coagulation indicators, inflammatory markers, and liver and kidney function indicators. To simulate the length of the extracorporeal circulation loop in the human body and increase the contact area between the catheter and blood, catheters with a length of 1.6 m and an inner diameter of 3 mm were employed in these experiments. (Fig. S8A). The results showed that after prolonged contact with blood, the control group exhibited increased formation of the prothrombin-fragment F1+2
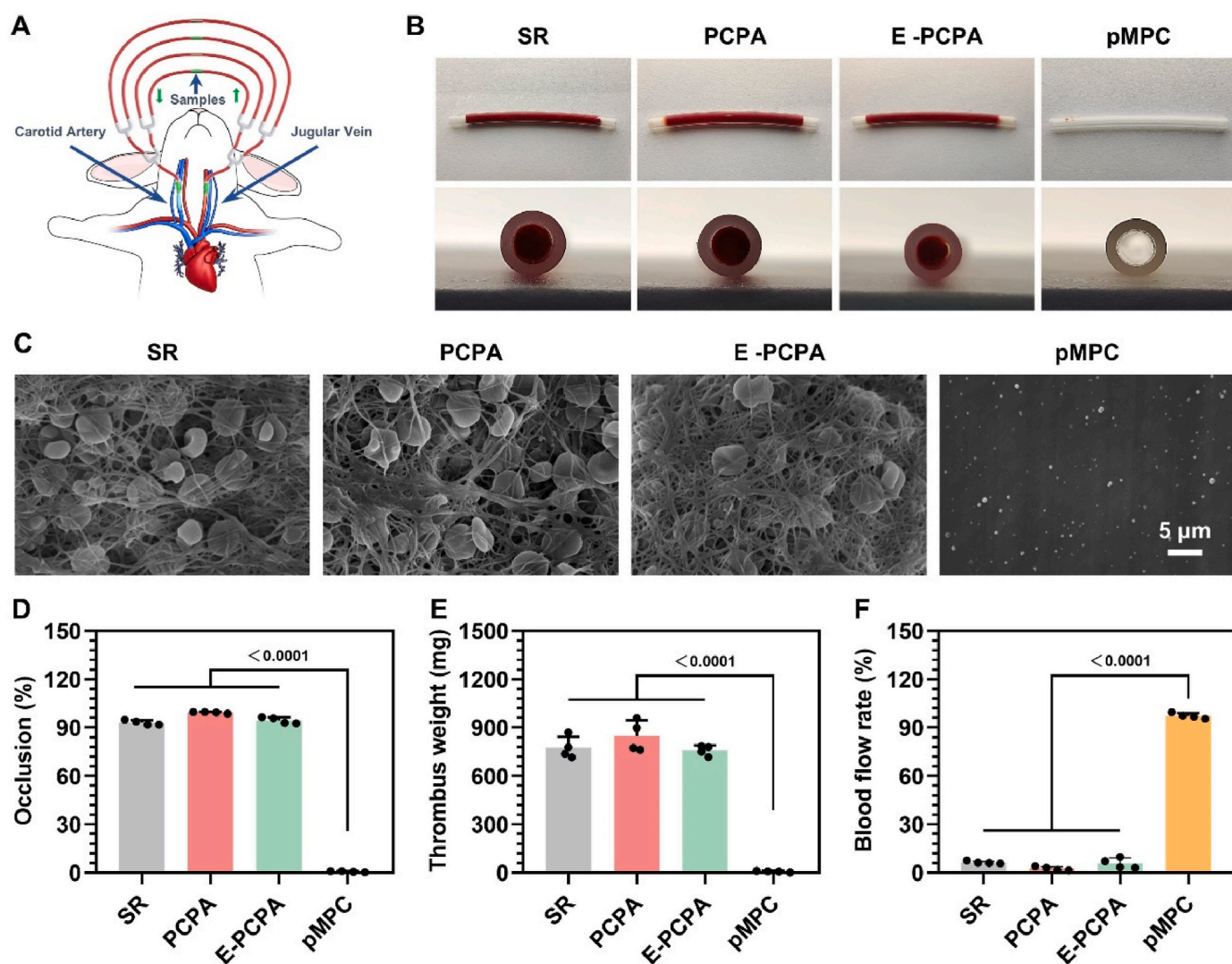
**Fig. 5.** Antithrombotic properties of pMPC armor *ex vivo*. (A) Schematic diagram of extracorporeal blood circulation experiment. (B) Images of side and cross-section view of different samples after blood circulation. (C) SEM images of the inside of the catheters after blood circulation (D) Occlusion rate, (E) thrombus weight, and (F) blood flow rate after blood circulation with bare and modified SR catheters. Data presented as mean ± SD (n = 4) and analysed using a one-way ANOVA.

(as marker of thrombin formation, Fig. S8B), indicating a higher coagulation tendency, while the pMPC group showed a decreased expression of F1+2. The decrease in APTT (Fig. S8C) and PLT (Fig. S8D) observed during the experimental time may be attributed to unavoidable injuries to the organism during the experiment. Additionally, the fact that the blood used for the test was taken from the catheter site may also affect the results of the test. However, there were no significant differences between the SR group and pMPC group.

The implantation of devices into the body can trigger the immune system, potentially causing an inflammatory reaction. However, there were no significant changes in inflammatory indicators for pMPC group, including C3a (Fig. S8E), CRP (Fig. S8F), WBC (Fig. S8G), IL-10 (Fig. S8H), and TNF-α (Fig. S8I), indicating that the inflammation was only mild or not induced. The increase in IL-10 of SR during the experimental time, possibly due to potential inflammatory response associated with SR.

To further examine the potential toxicity of our armor on liver and kidney tissues, the expression levels of ALT (Fig. S8J) and CREA (Fig. S8K) were measured. The results showed that both SR and pMPC-grafted surfaces did not cause liver or kidney function damage under dynamic circulation conditions. These findings demonstrated the biosafety of our pMPC armor.

## 3.5. Durability of antibacterial and antithrombogenic properties of the pMPC coating armor

According to patient needs, CVCs indwelling may be required for several days or even weeks, emphasizing the crucial importance of maintaining long-term effectiveness in catheter surface functionality. To assess the stability of pMPC, we exposed the catheters to PBS for different durations. ICP-MS analysis revealed that the phosphorus element content in the solution was gradually increased and reached 24.63 ppm after 30 days of immersion (Fig. 6A), indicating the degradation of poly-2-methacryloyloxyethyl phosphorylcholine. Meanwhile, after 15 and 30 days of PBS treatment, the coating thickness declined to 128.94 nm and 119.37 nm, respectively. Considering that the initial thickness of the E-PCPA coating was 65.03 nm, the thickness of the zwitterionic polymer armor remained at 54.34 nm after 30 days of immersion (Fig. 6B). Remarkably, after 15 days of immersion, the water contact angle on the dry pMPC surface was around 7°, and remained less than 20° even after 30 days of immersion (Fig. 6C). Research has shown that when the water contact angle is less than 20°, it has an effective inhibitory effect on non-specific adsorption of proteins [43]. These results indicate that the pMPC surface still exhibited excellent hydrophilicity even after 30 days of PBS treatment, implying the preservation of
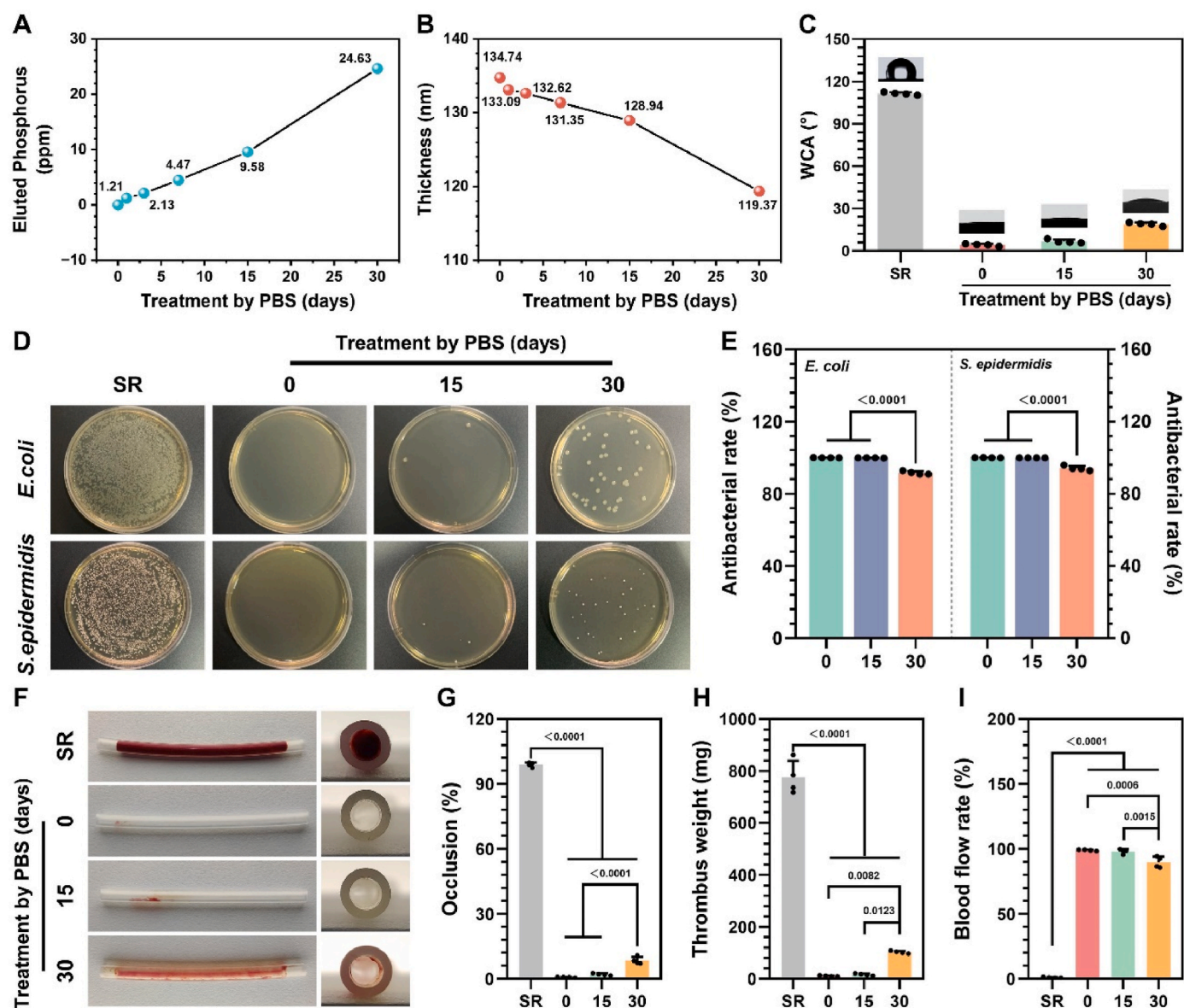
**Fig. 6.** Durability of antifouling properties of pMPC armor. (A) Thickness of pMPC armor on SR substrates after PBS treatment with different durations. (B) Phosphorus content eluted in PBS soaking solution (C) Water contact angle of pMPC surface after treatment for different days. (D) Typical *E. coli* and *S. epidermidis* colonies after 24 h incubation on pMPC surface after immersion with different days. Antibacterial rate of the immersed surface against (E) *E. coli* and *S. epidermidis*. (F) Photographs of side and cross-sectional of the pMPC-modified catheters before and after treatments by PBS for different durations. (G) Occlusion. (H) Thrombus weight. (I) Blood flow rate. Data presented as mean ± SD (n = 4) and analysed using a one-way ANOVA.

its antifouling properties.

To further verify the durability of the pMPC armored SR after PBS immersion, we first conducted an antibacterial test. The results showed that even after prolonged immersion for 30 days, the coating exhibited significant resistance to bacterial adhesion, maintaining an antibacterial rate above 90 % for both *E. coli* and *S. epidermidis* (Fig. 6D and E). To assess the antithrombotic properties of the pMPC surface, we conducted an *ex vivo* circulation experiment. After circulation, the unmodified SR catheter surface exhibited severe thrombus accumulation. However, the pMPC-armored catheter showed only little thrombus even after 30 days of PBS treatment (Fig. 6F). Quantitative results confirmed the stability and anti-thrombogenicity properties of pMPC armor. After 30 days of immersion, the pMPC-modified catheter showed no significant blockage, and the blood flow rate remained around 90 % (Fig. 6G–I), indicating the well-preserved antithrombotic function. These results suggested that, despite the pMPC surface underwent some degradation during PBS treatment, the retained polymer brushes still functioned

well, providing sustained preventive effects against microbial adhesion and thrombus accumulation.

### 3.6. In vivo antifouling properties of pMPC coating armored catheters

Encouraged by the results of *ex vivo* experiments and aiming to more realistically simulate clinical scenarios, two animal models, a rat subcutaneous infection model and a rabbit jugular vein model, were further performed to evaluate the antifouling efficacy of our armor. Firstly, for the rat subcutaneous infection model, we exposed both bare and modified CVCs to a $5 \times 10^6$–$1 \times 10^7$ CFU/mL microorganisms (*E. coli* or *S. epidermidis*) medium for 24 h. After treatment with physiological saline, the bacteria-contaminated samples were placed in pockets on the backs of healthy rats (Fig. 7A). After 7 days of implantation, the samples and surrounding tissues were harvested for HE staining. As shown in Fig. 7B and C, compared to unmodified CVCs, the pMPC-modified CVCs exhibited a significant reduction in the area of inflammatory cell
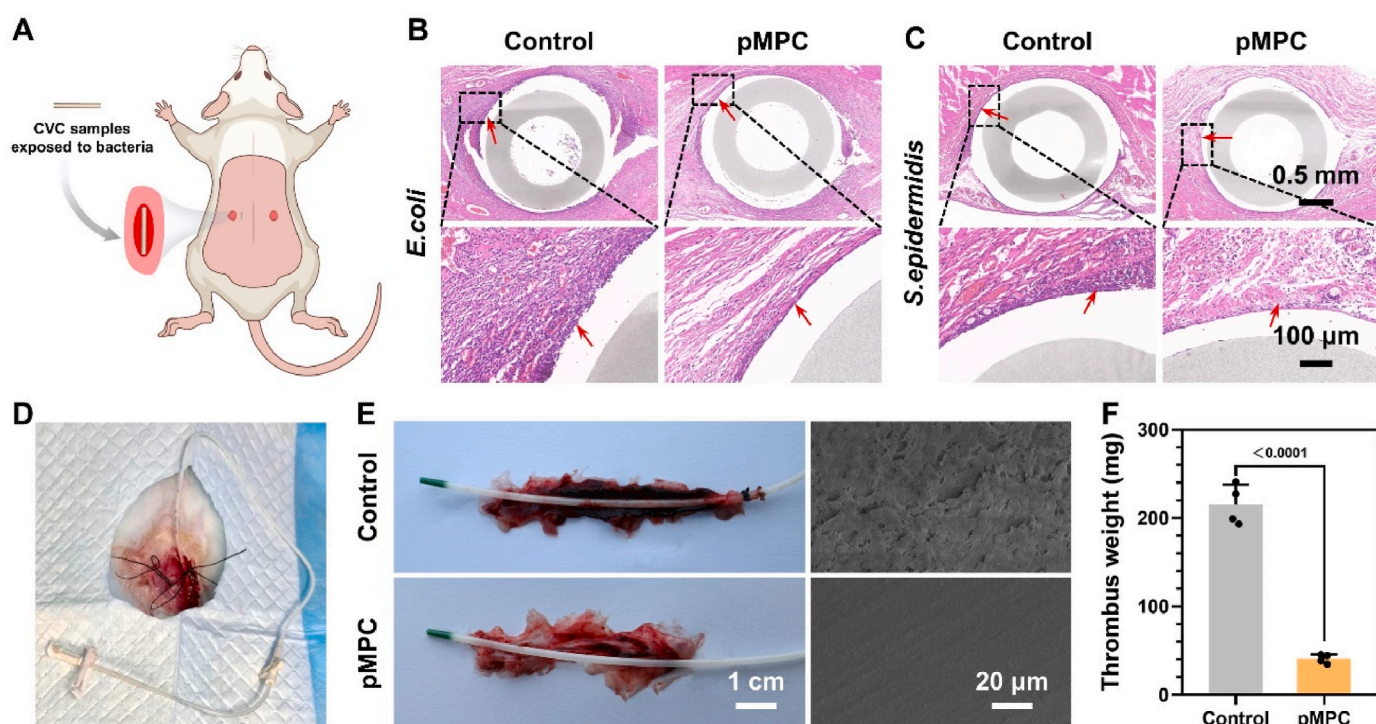
**Fig. 7.** (A) Schematic illustration for placement of CVCs in pockets on the backs of rats. H&E stained images of CVCs exposed to (B) *E. coli* and (C) *S. epidermidis*. Red arrows indicate inflammatory cell infiltration. (D) Schematic illustration image for insertion of CVCs into the rabbit jugular veins. (E) Surface morphology of CVCs. (F) Weight of thrombus formed on the surface CVCs. Data are presented as mean ± SD (n = 4) and statistical analysis was performed using a one-way ANOVA.

infiltration. This result confirms that the pMPC armored catheters not only possess biocompatibility but also alleviate inflammation responses by eradicating bacterial infections around the implantation site.

To assess the *in vivo* thrombogenicity of pMPC-modified CVCs, we utilized a rabbit jugular vein model. We compared the performance of pMPC-modified CVCs and clinically used CVCs by implanting them into the jugular veins of adult New Zealand white rabbits (Fig. 7D). After 8 h of implantation, the exterior of the clinically used CVCs exhibited significant thrombus accumulation (Fig. 7E). In contrast, the pMPC-coated CVCs showed little thrombus between the surface and surrounding vessel walls. SEM observation further confirmed this, as the surface of bare CVCs showed a noticeable fibrous network, while the surface of the catheter modified with zwitterionic polymers exhibited little adherence of blood components. Quantitative results indicated a significant 81 % reduction in thrombus formation on the surface of pMPC-modified CVCs (Fig. 7F). These results illustrated that the pMPC armor can effectively prevent the accumulation of acute thrombosis under *in vivo* conditions.

## 4. Conclusion

In this work, we developed a super-hydrophilic zwitterionic polymer armor for endowing CVCs with excellent antibacterial and anticoagulant capabilities. To achieve this, we first fabricate a robust, amine-rich PCPA coatings through insect sclerotization-inspired phenol-polyamine chemistry. Subsequently, the zwitterionic molecule MPC was applied to impart super-hydrophilicity to the catheters. Such a super-hydrophilic surface effectively prevents adhesion against bacteria, fibrinogen, and platelets *in vitro*, and inhibits clot formation in *ex vivo* circulation. Furthermore, the armored catheters retain their antibacterial and anticoagulant capabilities even after 30 days of immersion in PBS. In practical applications, our armor proves effective in regulating inflammation in a rat subcutaneous model and inhibiting coagulation in a rabbit model. Overall, our approach presents a promising solution for reducing infection and thrombosis in associated with catheters.

## Data availability statement

The data that support the findings of this study are available from the corresponding authors upon reasonable request.

## CRediT authorship contribution statement

**You Ke:** Writing – original draft, Methodology, Investigation. **Haotian Meng:** Visualization, Investigation, Formal analysis, Data curation. **Zeyu Du:** Methodology, Formal analysis, Data curation, Conceptualization. **Wentai Zhang:** Writing – review & editing, Supervision, Formal analysis. **Qing Ma:** Resources, Methodology, Formal analysis. **Yuting Huang:** Visualization, Investigation. **Linxian Cui:** Writing – review & editing, Supervision, Methodology. **Yifeng Lei:** Writing – review & editing, Supervision, Methodology. **Zhilu Yang:** Writing – review & editing, Supervision, Resources, Funding acquisition, Conceptualization.

## Declaration of generative AI and AI-assisted technologies in the writing process

During the preparation of this work the author used ChatGPT 3.5 in order to polish the language of the article. After using this ChatGPT 3.5, the author(s) reviewed and edited the content as needed and take(s) full responsibility for the content of the publication.

## Declaration of competing interest

Prof. Zhilu Yang is an editorial board member for Bioactive Materials and was not involved in the editorial review or the decision to publish this article. All authors declare that there are no competing interests.

## Acknowledgments

Institute for Polymer Research, Dresden) for checking the article and his valuable comments. This work was supported by the National Natural Science Foundation of China (Project 82072072, 32261160372, 32171326, 32371377), the Guangdong Basic and Applied Basic Research Foundation (2022B1515130010, 2021A1515111035), Dongguan Science and Technology of Social Development Program (20231800906311, 20231800900332).

## Appendix A. Supplementary data

Supplementary data to this article can be found online at https://doi.org/10.1016/j.bioactmat.2024.04.002.

## References

[1] D.C. McGee, M.K. Gould, Preventing complications of central venous catheterization, N. Engl. J. Med. 348 (12) (2003) 1123–1133, https://doi.org/10.1056/NEJMra011883.

[2] N.S. Reston, P.N. Jerry, Central venous catheters, Br. Med. J. 347 (2013) 6570–6580, https://doi.org/10.1136/bmj.f6570.

[3] M. Gallieni, I. Brenna, F. Brunini, N. Mezzina, S. Pasho, A. Giordano, Dialysis central venous catheter types and performance, J. Vasc. Access 15 (7_suppl) (2014) 140–146, https://doi.org/10.5301/jva.5000262.

[4] R.E. Kusminsky, Complications of central venous catheterization, J. Am. Coll. Surg. 204 (4) (2007) 681–696, https://doi.org/10.1016/j.jamcollsurg.2007.01.039.

[5] X. Mou, H. Zhang, H. Qiu, W. Zhang, Y. Wang, K. Xiong, N. Huang, H.A. Santos, Z. Yang, Mussel-Inspired and Bioclickable Peptide Engineered Surface to Combat Thrombosis and Infection, Research, 2022, pp. 1–14, https://doi.org/10.34133/2022/9780879.

[6] S. Fuchs, A. Pollak, D. Gilon, Central venous catheter mechanical irritation of the right atrial free wall:A cause for thrombus formation, Cardiology 91 (3) (1999) 169–172, https://doi.org/10.1159/000006905.

[7] B. Niemann, L. Dudas, D. Gray, A. Pettit, A. Wilson, J.M. Bardes, Biofilm Formation on central venous catheters: a pilot study, J. Surg. Res. 280 (2022) 123–128, 0.1016/j.jss.2022.06.072.

[8] M. Gominet, F. Compain, C. Beloin, D. Lebeaux, Central venous catheters and biofilms: where do we stand in 2017? APMIS 125 (4) (2017) 365–375, https://doi.org/10.1111/apm.12665.

[9] R.S. Arora, R. Roberts, T.O. Eden, B. Pizer, Interventions other than anticoagulants and systemic antibiotics for prevention of central venous catheter-related infections in children with cancer, Cochrane Database Syst. Rev. 12 (2010) 1–11, https://doi.org/10.1002/14651858.CD007785.pub2.

[10] C.H. van den Bosch, J. van Woensel, M.D. van de Wetering, Prophylactic antibiotics for preventing gram-positive infections associated with long-term central venous catheters in adults and children receiving treatment for cancer, Cochrane Database Syst. Rev. (10) (2021) 1–39, https://doi.org/10.1002/14651858.CD003295.pub4.

[11] G.M. Arepally, T.L. Ortel, Heparin-induced thrombocytopenia, N. Engl. J. Med. 61 (2010) 77–90, https://doi.org/10.1056/NEJMcp052967.

[12] V. Pitiriga, P. Kanellopoulos, I. Bakalis, E. Kampos, I. Sagris, G. Saroglou, A. Tsakris, Central Venous Catheter-Related Bloodstream Infection and Colonization: the Impact of Insertion Site and Distribution of Multidrug-Resistant Pathogens, Antimicrob. Resist. in., vol. 9, 2020, pp. 1–8, https://doi.org/10.1186/s13756-020-00851-1.

[13] Y. Wu, H. Wang, P.K. Chu, Enhancing macrophages to combat intracellular bacteria, The Innovation Life 1 (2) (2023) 100027–100028, https://doi.org/10.59717/j.xinn-life.2023.100027.

[14] S. Zhang, H. Yang, M. Wang, D. Mantovani, K. Yang, F. Witte, L. Tan, B. Yue, X. Qu, Immunomodulatory biomaterials against bacterial infections: progress, challenges, and future perspectives, Innovation 4 (6) (2023) 100503–1005015, https://doi.org/10.1016/j.xinn.2023.100503.

[15] R.S. Smith, Z. Zhang, M. Bouchard, J. Li, H.S. Lapp, G.R. Brotske, D.L. Lucchino, D. Weaver, L.A. Roth, A. Coury, J. Biggerstaff, S. Sukavaneshvar, R. Langer, C. Loose, Vascular catheters with a nonleaching poly-sulfobetaine surface modification reduce thrombus formation and microbial attachment, Sci. Transl. Med. 4 (153) (2012) 132–141, https://doi.org/10.1126/scitranslmed.3004120.

[16] J. Valtin, S. Behrens, A. Ruland, F. Schmieder, F. Sonntag, L.D. Renner, M.F. Maitz, C. Werner, A new in vitro blood flow model for the realistic evaluation of antimicrobial surfaces, Adv. Healthcare Mater. 12 (28) (2023) 2301300–2301310, https://doi.org/10.1002/adhm.202301300.

[17] U. Sjöbring, U. Ringdahl, Z.M. Ruggeri, Induction of platelet thrombi by bacteria and antibodies, Blood 100 (13) (2002) 4470–4477, https://doi.org/10.1182/blood-2002-01-0069.

[18] C.M. Faustino, S.M. Lemos, N. Monge, I.A. Ribeiro, A scope at antifouling strategies to prevent catheter-associated infections, Adv. Colloid Interface Sci. 284 (2020) 102230–102254, https://doi.org/10.1016/j.cis.2020.102230.

[19] W. Zhang, L. Cui, C. Xie, Z. Du, X. Mou, Y. Ke, Q. Ma, W. Tian, Z. Yang, Glycocalyx-inspired dynamic antifouling surfaces for temporary intravascular devices,

Biomaterials (2023) 122427–122441, https://doi.org/10.1016/j.biomaterials.2023.122427.

[20] A. Wallace, H. Albadawi, N. Patel, A. Khademhosseini, Y.S. Zhang, S. Naidu, G. Knuttinen, R. Oklu, Anti-fouling strategies for central venous catheters, cardiovasc diagn, Therapy 7 (Suppl 3) (2017) 246–257, https://doi.org/10.21037/cdt.2017.09.18.

[21] J. Baggerman, M.M. Smulders, H. Zuilhof, Romantic surfaces: a systematic overview of stable, biospecific, and antifouling zwitterionic surfaces, Langmuir 35 (5) (2019) 1072–1084, https://doi.org/10.1021/acs.langmuir.8b03360.

[22] S. Yao, H. Yan, S. Tian, R. Luo, Y. Zhao, J. Wang, Anti-fouling coatings for blood-contacting devices, Smart Mater. Med. 5 (1) (2024) 166–180, https://doi.org/10.1016/j.smaim.2023.10.001.

[23] M. He, K. Gao, L. Zhou, Z. Jiao, M. Wu, J. Cao, X. You, Z. Cai, Y. Su, Z. Jiang, Zwitterionic materials for antifouling membrane surface construction, Acta Biomater. 40 (2016) 142–152, https://doi.org/10.1016/j.actbio.2016.03.038.

[24] C. Leng, S. Sun, K. Zhang, S. Jiang, Z. Chen, Molecular level studies on interfacial hydration of zwitterionic and other antifouling polymers in situ, Acta Biomater. 40 (2016) 6–15, https://doi.org/10.1016/j.actbio.2016.02.030.

[25] D. Li, Q. Wei, C. Wu, X. Zhang, Q. Xue, T. Zheng, M. Cao, Superhydrophilicity and strong salt-affinity: zwitterionic polymer grafted surfaces with significant potentials particularly in biological systems, Adv. Colloid Interface Sci. 278 (2020) 102141–102158, https://doi.org/10.1016/j.cis.2020.102141.

[26] C. Wu, Y. Zhou, H. Wang, J. Hu, X. Wang, Formation of antifouling functional coating from deposition of a zwitterionic-Co-nonionic polymer via "grafting to" approach, J. Saudi Chem. Soc. 23 (8) (2019) 1080–1089, https://doi.org/10.1016/j.jscs.2019.05.011.

[27] L.D. Blackman, P.A. Gunatillake, P. Cass, K.E. Locock, An introduction to zwitterionic polymer behavior and applications in solution and at surfaces, Chem. Soc. Rev. 48 (3) (2019) 757–770, https://doi.org/10.1039/C8CS00508G.

[28] B. Yu, J. Zheng, Y. Chang, M. Sin, C. Chang, A. Higuchi, Y. Sun, Surface zwitterionization of titanium for a general bio-inert control of plasma proteins, blood cells, tissue cells, and bacteria, Langmuir 30 (25) (2014) 7502–7512, https://doi.org/10.1021/la500917s.

[29] M.S.H. Akash, K. Rehman, M.S.H. Akash, K. Rehman, Ultraviolet-visible (Uv-Vis) spectroscopy, Essentials of Pharmaceutical Analysis (2020) 29–56. https://link.springer.com/chapter/10.1007/978-981-15-1547-7_3.

[30] W. Feng, J.L. Brash, S. Zhu, Non-biofouling materials prepared by atom transfer radical polymerization grafting of 2-methacryloloxyethyl phosphorylcholine: separate effects of graft density and chain length on protein repulsion, Biomaterials 27 (6) (2006) 847–855, https://doi.org/10.1016/j.biomaterials.2005.07.006.

[31] R. Iwata, P. Suk-In, V.P. Hoven, A. Takahara, K. Akiyoshi, Y. Iwasaki, Control of nanobiointerfaces generated from well-defined biomimetic polymer brushes for protein and cell manipulations, Biomacromolecules 5 (6) (2004) 2308–2314, https://doi.org/10.1021/bm049613k.

[32] Z. Wang, J. Li, Y. Liu, J. Luo, Macroscale superlubricity achieved between zwitterionic copolymer hydrogel and sapphire in water, Mater. Des. 188 (2020) 108441–108449, https://doi.org/10.1016/j.matdes.2019.108441.

[33] A.B. Wysocki, Evaluating and managing open skin wounds: colonization versus infection, AACN Adv. Crit. Care 13 (3) (2002) 382–397, https://doi.org/10.1097/00044067-200208000-00005.

[34] Z. Yuan, L. Zhang, S. Jiang, M. Shafiq, Y. Cai, Y. Chen, J. Song, X. Yu, H. Ijima, Y. Xu, Anti-inflammatory, antibacterial, and antioxidative bioactive glass-based nanofibrous dressing enables scarless wound healing, Smart mater. Med. 4 (2023) 407–426, https://doi.org/10.1016/j.smaim.2023.01.001.

[35] M. Sun, J. Dong, Y. Xia, R. Shu, Antibacterial activities of docosahexaenoic acid (dha) and eicosapentaenoic acid (epa) against planktonic and biofilm growing Streptococcus mutans, Microb. Pathog. 107 (2017) 212–218, https://doi.org/10.1016/j.micpath.2017.03.040.

[36] S. Kattula, J.R. Byrnes, A.S. Wolberg, Fibrinogen and fibrin in hemostasis and thrombosis, Arterioscler. Thromb. Vasc. Biol. 37 (3) (2017) 13–21, https://doi.org/10.1161/ATVBAHA.117.308564.

[37] Y.K. Sung, D.R. Lee, D.J. Chung, Advances in the development of hemostatic biomaterials for medical application, Research 25 (1) (2021) 37, https://doi.org/10.1186/s40824-021-00239-1.

[38] P. Żeliszewska, A. Bratek-Skicki, Z. Adamczyk, M. Cieśla, Human fibrinogen adsorption on positively charged latex particles, Langmuir 30 (37) (2014) 11165–11174, https://doi.org/10.1021/la5025668.

[39] S. Uitte de Willige, K.F. Standeven, H. Philippou, R.A. Ariëns, The pleiotropic role of the fibrinogen γ′ chain in hemostasis, Blood 114 (19) (2009) 3994–4001, https://doi.org/10.1182/blood-2009-05-217968.

[40] Y. Sang, M. Roest, B. de Laat, P.G. de Groot, D. Huskens, Interplay between platelets and coagulation, Blood Rev. 46 (2021) 100733–100743, https://doi.org/10.1016/j.blre.2020.100733.

[41] D. Boraschi, A. Tagliabue, Harnessing the power of inflammation in immunoprevention and immunotherapy, The Innovation Life 1 (2) (2023) 100025, https://doi.org/10.59717/j.xinn-life.2023.100025.

[42] I.H. Jaffer, J.I. Weitz, The blood compatibility challenge. Part 1: blood-contacting medical devices: the scope of the problem, Acta Biomater. 94 (2019) 2–10, https://doi.org/10.1016/j.actbio.2019.06.021.

[43] E.A. Vogler, Protein adsorption in three dimensions, Biomaterials 33 (5) (2012) 1201–1237, https://doi.org/10.1016/j.biomaterials.2011.10.059.